

Dalton Transactions

Accepted Manuscript



This is an *Accepted Manuscript*, which has been through the Royal Society of Chemistry peer review process and has been accepted for publication.

Accepted Manuscripts are published online shortly after acceptance, before technical editing, formatting and proof reading. Using this free service, authors can make their results available to the community, in citable form, before we publish the edited article. We will replace this *Accepted Manuscript* with the edited and formatted *Advance Article* as soon as it is available.

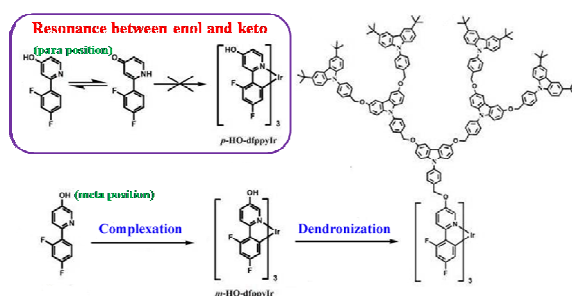
You can find more information about *Accepted Manuscripts* in the [Information for Authors](#).

Please note that technical editing may introduce minor changes to the text and/or graphics, which may alter content. The journal's standard [Terms & Conditions](#) and the [Ethical guidelines](#) still apply. In no event shall the Royal Society of Chemistry be held responsible for any errors or omissions in this *Accepted Manuscript* or any consequences arising from the use of any information it contains.

Graphical Abstract

Synthesis and Properties of Blue-Emitting Iridium Dendrimers with N-phenylcarbazole-Based Polyether Dendrons by a Post-Dendronization Route

Yang Wang,^{†,‡} Shumeng Wang,^{†,‡} Shiyang Shao,[†] Junqiao Ding,^{*,†} Lixiang Wang,^{*,†} Xiabin Jing,[†] and Fosong Wang[†]



A series of solution processible blue-emitting Ir dendrimers with N-phenylcarbazole based polyether dendrons have been developed via a convenient post-dendronization procedure. It involves the successful preparation of *m*-HO-dfppyIr with the reactive hydroxyl group at the meta position so as to eliminate the possible resonance structure between enol and keto, followed by the subsequent dendronization. Compared with the previously used method, this strategy is more effective for the synthesis of multifunctional Ir dendrimers since it can be easily extended to different cores and periphery dendrons.

Cite this: DOI: 10.1039/c0xx00000x

www.rsc.org/xxxxxx

ARTICLE TYPE

Synthesis and Properties of Greenish-Blue-Emitting Iridium Dendrimers with N-phenylcarbazole-Based Polyether Dendrons by A Post-Dendronization Route

Yang Wang^{a,b}, Shumeng Wang^{a,b}, Shiyang Shao^a, Junqiao Ding^{a,*}, Lixiang Wang^{a,*}, Xiabin Jing^a, and Fosong Wang^a

Received (in XXX, XXX) Xth XXXXXXXXX 20XX, Accepted Xth XXXXXXXXX 20XX

DOI: 10.1039/b000000x

Abstract: A series of solution processible greenish-blue-emitting Ir dendrimers with polyether dendrons that consist of N-phenylcarbazole (NPC) have been developed via a convenient post-dendronization method. It involves two steps: i) the successful preparation of a reactive Ir core, namely *m*-HO-dfppyIr, only when the hydroxyl group locates at the meta position relative to N atom in the C^N ligand so as to eliminate the possible resonance structure between enol and keto; and ii) the subsequent functionalization with NPC-based polyether dendrons to afford the first, second and third generation Ir dendrimers (**Ir-G1B**, **Ir-G2B** and **Ir-G3B**) with ease and high yields over 60%. All these dendritic complexes possess good thermal stability with decomposition temperatures higher than 380 °C and glass transition temperatures higher than 200 °C. In addition, with the growing generation number, the intermolecular interactions between emissive Ir cores are expected to be effectively inhibited to avoid the luminescence quenching, which is confirmed by the blue-shifted emission peak and enhanced lifetime of **Ir-G3B** in solid states. As a result, on going from **Ir-G1B** to **Ir-G3B**, the maximum luminous efficiency moves upward from 4.7 to 9.2 cd/A for nondoped electrophosphorescent devices. Further optimization by doping them into a dendritic H2 host leads to the improved luminous efficiencies as high as 20.0-25.2 cd/A.

Introduction

Phosphorescent organic light-emitting diodes (PhOLEDs) with transition metal-containing materials, especially iridium (Ir) complexes, have attracted extensive attention owing to their capability to harvest both singlet and triplet excitons to realize a theoretical internal quantum efficiency of 100%.¹⁻⁷ In a traditional fabrication process of PhOLEDs, Ir complexes together with suitable host matrixes are often deposited thermally to form uniform emissive layers.⁸⁻¹³ This technology is high-cost including considerable waste of functional materials, and heavy time and energy consumption. Therefore, it is desirable to develop Ir complexes suitable for low-cost solution processes, such as inkjet printing and spin-coating. To obtain this object, one promising approach is physically or chemically doping an Ir complex into a polymeric host.¹⁴⁻¹⁸ However, the multidispersed structure and batch-to-batch variation, characteristic of a polymer system, inevitably lead to unsatisfactory device performance compared with vacuum-deposited PhOLEDs.

Phosphorescent dendrimers that consist of an emissive Ir core encapsulated by periphery dendrons have emerged as an alternative to solution processible triplet emitters since they combine the well-defined structure of small molecules with good solution processibility of polymers.¹⁹⁻²¹ According to the nature of dendrons, generally, the dendritic Ir complexes can be

categorized into two classes: those that contain electrically insulating dendrons (phenylene,²²⁻²⁴ Fréchet²⁵ and Müllen dendrons²⁶ etc.), and those that contain electroactive dendrons (triphenylamine²⁷⁻³⁰ and carbazole dendrons³¹⁻³⁴ etc.) to improve charge injection and transport capacities.³⁵ We note that most of them are synthesized by a pre-dendronization method, which involves the preparation of dendronized ligands followed by subsequent coordination with Ir salts (Fig. 1). This route is not compatible with large dendrons due to their poor solubility in widely-used polar solvent system (glycerol and diglymer etc.), resulting in incomplete complexation and low yield³¹. Moreover, the degree of freedom seems to be very low when the dendron and core are modified to construct different Ir dendrimers with various optoelectronic properties.

In this work, we report a post-dendronization strategy for the convenient synthesis of solution processible greenish-blue-emitting Ir dendrimers with polyether dendrons made of N-phenylcarbazole (NPC). As outlined in Scheme 1, two steps are involved: 1) A reactive Ir core with three hydroxy groups, namely *m*-HO-dfppyIr other than *p*-HO-dfppyIr, is firstly synthesized for the possible existed resonance structure between enol and keto induced by the hydroxyl position has a great effect on the complexation; 2) *m*-HO-dfppyIr is then readily combined with the NPC-based polyether dendrons³⁶ to afford the first, second and third generation Ir dendrimers (Ir-G1B, Ir-G2B and Ir-G3B)

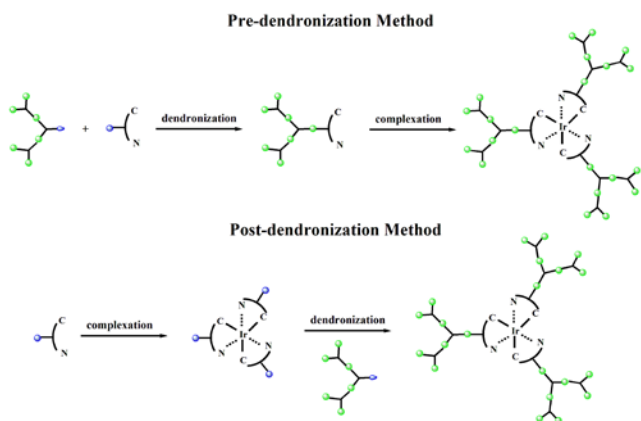


Fig. 1 Two methods for the preparation of Ir-cored dendrimers.

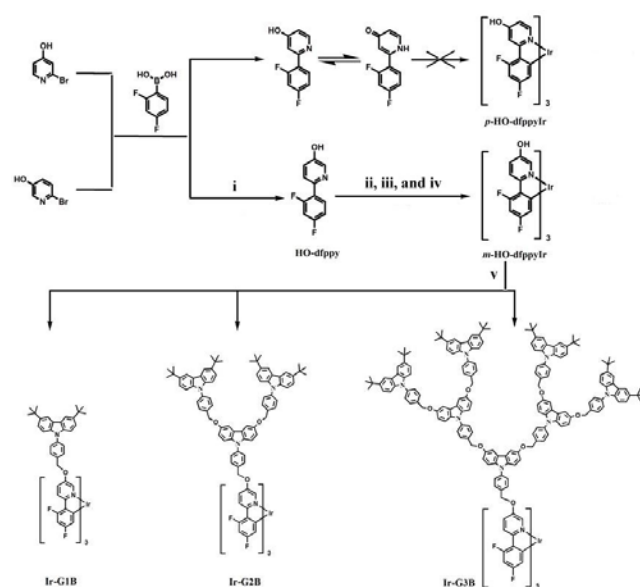
in high yields over 60%. With these easily-obtained Ir dendrimers in hand, their photophysical, electrochemical and electroluminescent (EL) properties are investigated in detail.

Results and discussion

Synthesis and characterization

Different from pre-dendronization, a post-dendronization procedure involves the preparation of an emissive Ir core functionalized with reactive groups, which subsequently reacts with the periphery dendron to give the final dendritic complex (Fig. 1). Obviously, the success of this method is dependent on the first step. So we at first tried to prepare *p*-HO-dfppyIr with three hydroxyl groups at the para position relative to N atom, but failed (Scheme 1). The failure could be reasonably ascribed to the possible resonance structure between enol and keto, which would further weaken the coordination ability of N atom in the C^N ligand. To eliminate this negative effect, we then tuned the position of hydroxyl group from para to meta, and successfully obtained the desired intermediate *m*-HO-dfppyIr with three hydroxyl groups at the meta position relative to N atom. Noticeably, the direct product of *m*-HO-dfppyIr, synthesized via a modified two-step reaction, has a dominant meridional configuration showing three sets of ¹H NMR signals (Fig. 2). Under exposure to a 125 W UV light, it could be completely converted to the facial isomer with only one set of signals³⁷. In addition, the existed sharp peak at about 10.39 ppm is an indicator of the reactive hydroxyl groups.

Together with the NPC-based polyether dendrons that have the advantages of the ease of synthesis and electroactive function³⁶, finally, *m*-HO-dfppyIr was post-dendronized to produce a series of solution processible greenish-blue-emitting Ir dendrimers **Ir-G1B**, **Ir-G2B** and **Ir-G3B** in high yields of 60-70%. After the completion of the reaction, the 10.39 ppm signal corresponding to the hydroxyl group is found to vanish, and a singlet characteristic peak of the NPC moiety in the periphery dendrons appears at 8.11 ppm (Fig. 2). Moreover, the resultant Ir dendrimers display only one simple set of signals in their ¹H NMR spectra as the facial isomer *m*-HO-dfppyIr does, indicating that the configuration of the complex is not influenced by the post-dendronization. The chemical structures of all the dendrimers were further confirmed by ¹⁹F NMR spectroscopy, elemental



Reagents and conditions: (i) Pd(PPh₃)₄, Na₂CO₃(aq), THF, 70 °C; (ii) Iridium(III) chloride trihydrate, water, 2-methoxyethanol, reflux; (iii) silver trifluoroacetate, HO-dfppy, 2-ethoxyethanol, reflux; (iv) 125 W UV light, methanol; (v) **Dn-Br** (n = 1, 2 and 3), Cs₂CO₃, DMF, 100 °C.

analysis, and matrix-assisted laser desorption-ionization time-of-flight (MALDI-TOF) mass spectrometry.

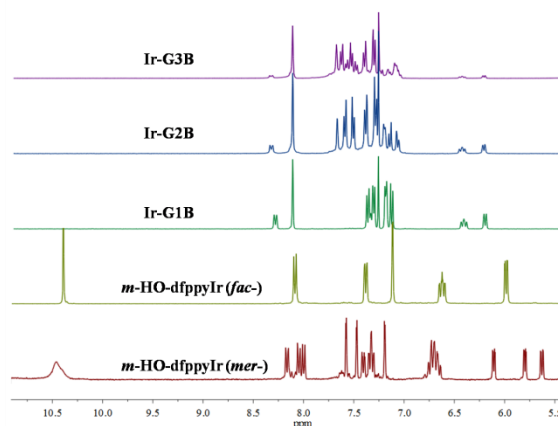


Fig. 2 The part of ¹H NMR spectra of *m*-HO-dfppyIr and its corresponding Ir dendrimers.

Thermal Properties

The thermal properties of the dendrimers **Ir-G1B**, **Ir-G2B** and **Ir-G3B** were investigated by thermogravimetric analysis (TGA) and differential scanning calorimetry (DSC) at a scanning rate of 10 °C min⁻¹ under nitrogen atmosphere. As shown in Fig. 3a, all the dendrimers are thermally stable with decomposition temperatures (T_d: at a 5% weight loss) higher than 380 °C. They also show high glass transition temperatures (T_g) above 200 °C (Fig. 3b). For example, **Ir-G1B** exhibits a T_g of 221 °C, and it is slightly increased to 242 °C for **Ir-G3B** with the growing generation. The high T_gs allow their films formed by spin-coating to be morphologically stable, which is favorable for the long-term reliability of the devices.

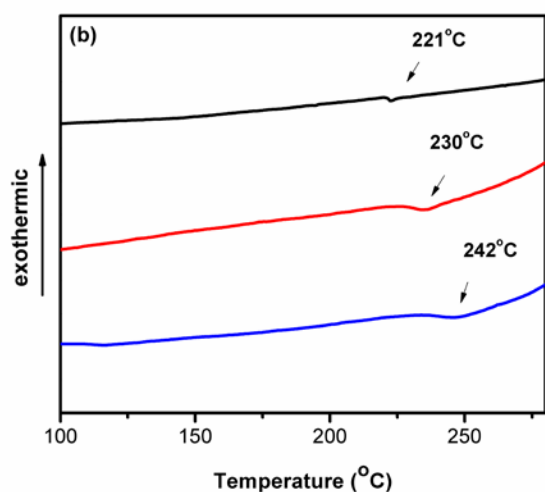
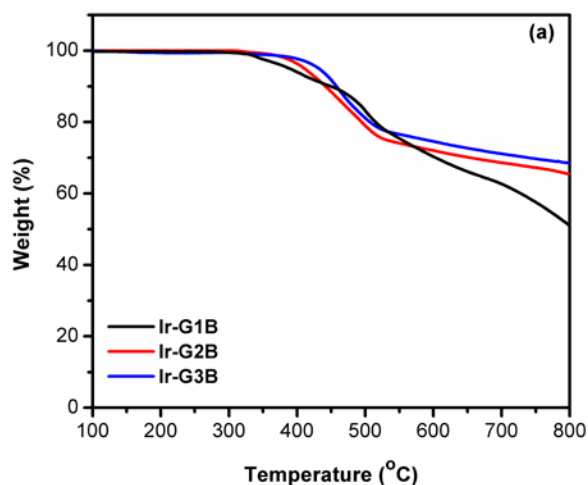


Fig. 3 TGA (a) and DSC curves (b) for Ir dendrimers.

Photophysical and electrochemical properties

The UV-vis absorption spectra in CH_2Cl_2 and photoluminescence (PL) spectra in toluene of the dendrimers are shown in Fig. 4a, and the data are tabulated in Table 1. The strong absorption bands below 380 nm are attributed to the spin-allowed $\pi-\pi^*$ transitions of the C^N ligand 2-(2,4-difluorophenyl)pyridine as well as polyether dendrons containing NPC moieties. As the number of NPC increases, the intensity of the characteristic bands at 298/310/347/370 nm increases gradually, which is consistent with our previous report³⁶. Meanwhile, the weak bands in the range of 380-460 nm are assigned to the metal-to-ligand charge-transfer (MLCT) transitions of the emissive Ir core *m*-HO-dfppyIr.

As one can see from Fig. 4a, the PL spectra of the dendrimers in solutions remain nearly unchanged since they all show well-resolved emissions from the Ir core with peaks at 483 nm and shoulders at 500 nm. On going from solutions to solid states, the emission maxima move towards a longer wavelength from 483 nm to 507-513 nm, indicative of aggregation to some degree. The observed red-shifts are 30, 27 and 24 nm for Ir-G1B, Ir-G2B and Ir-G3B, respectively. With the growing generation, the

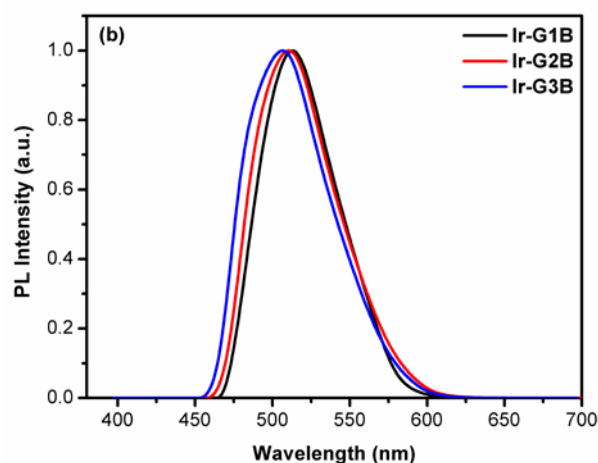
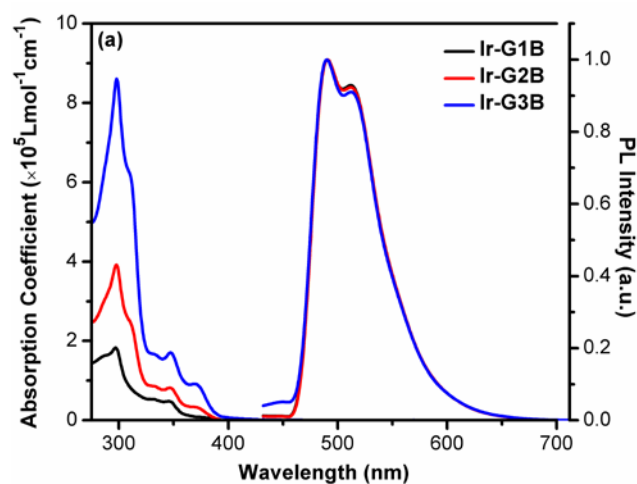


Fig. 4 UV-vis absorption and PL spectra in solutions (a), and PL spectra in thin films (b) for Ir dendrimers.

diminished bathochromic effect implies that the intermolecular interactions between emissive Ir cores can be prevented because of the encapsulation from dendrons. In fact, when the periphery dendrons become larger, the emissive Ir cores could be isolated more and more effectively, thereby avoiding the quenching of the

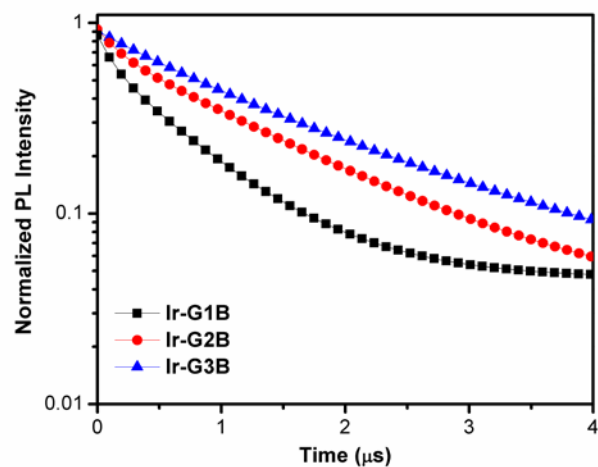


Fig. 5 The decay of the PL intensity for Ir dendrimers in films measured under argon atmosphere ($\lambda_{\text{ex}} = 355 \text{ nm}$).

Cite this: DOI: 10.1039/c0xx00000x

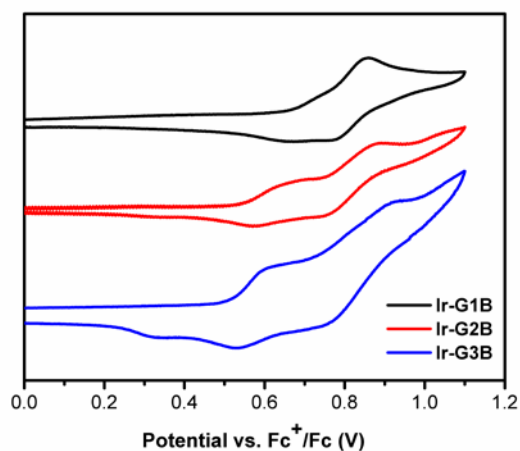
www.rsc.org/xxxxxxx

ARTICLE TYPE

Table 1. Photophysical, electrochemical, and thermal properties of Ir dendrimers.

	λ_{abs} (log ϵ) ^a [nm]	λ_{em} ^b [nm]	λ_{em} ^c [nm]	Φ_{p} ^d	τ ^c [μs]	ΔE_{g} ^e [eV]	HOMO/LUMO ^f [eV]	T_{d} [°C]	T_{g} [°C]
Ir-G1B	298 (5.2), 347 (4.7), 388 (3.6), 432 (3.0), 460 (2.1)	483, 500	513	0.41	0.64	2.64	-5.47/-2.83	389	221
Ir-G2B	298 (5.6), 310 (5.4), 347 (4.9), 369 (4.5), 388 (3.8), 431 (3.2), 460 (2.2)	483, 500	510	0.50	1.25	2.64	-5.34/-2.70	412	230
Ir-G3B	298 (5.9), 309 (5.7), 347 (5.2), 370 (4.9), 390 (4.1), 432 (3.2), 460 (2.2)	483, 500	507	0.46	1.56	2.64	-5.32/-2.68	432	242

^a Measured in CH_2Cl_2 at 298 K at a concentration of 10^{-6} M. ϵ is the absorption coefficient in the Lambert–Beer equation; ^b Measured in toluene at 298 K at a concentration of 10^{-5} M; ^c Measured in thin films at 298 K; ^d Measured in degassed toluene relative to *fac*-Ir(ppy)₃ ($\Phi = 0.40$); ^e ΔE_{g} : the optical band gap estimated from the onset of the absorption edge; ^f HOMO = -e [$E_{\text{ox}} + 4.8$ V], LUMO = HOMO + ΔE_{g} , where E_{ox} is taken from the onset of the oxidation potential.

**Fig. 6** CV curves of Ir dendrimers.

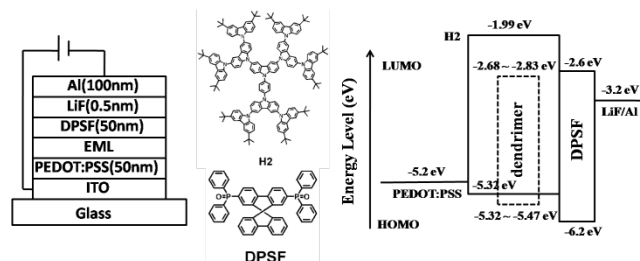
luminescence. To further confirm this, the film transient PL spectra of the dendrimers were measured. As depicted in Fig. 5, **Ir-G3B** with the third generation dendron decays much slower than **Ir-G1B** and **Ir-G2B**. And the average lifetime, estimated from a biexponential fit of emission decay curve, is up from 0.64 μs of **Ir-G1B** to 1.25 μs of **Ir-G2B** and 1.56 μs of **Ir-G3B**.

Cyclic voltammetry (CV) was used to characterize the electrochemical properties of the dendrimers. They all display multiple oxidation behavior coming from both the Ir core and NPC-based polyether dendrons (Fig. 6). As for **Ir-G1B**, the first oxidation located at 0.67 eV can be assigned to *m*-HO-dfppyIr, while the second one (0.72 eV) originates from the outer NPC capped with *tert*-butyl groups. Apart from them, a novel oxidation process appears at a more negative potential of 0.54 eV for **Ir-G2B** and **Ir-G3B**, which is from the inner NPC with alkyloxy substituents³⁶. According to the onset of the first oxidation potential, the highest occupied molecular orbital (HOMO) energy levels are calculated to be -5.47 eV, -5.34 eV

and -5.32 eV for **Ir-G1B**, **Ir-G2B** and **Ir-G3B**, respectively. Compared with **Ir-G1B**, the elevated HOMO levels of **Ir-G2B** and **Ir-G3B** are expected to reduce the hole injection barrier, and thus improve the device performance.

30 Electroluminescent properties

To evaluate the dendrimers as the potential solution processible phosphors, nondoped PhOLEDs with a configuration of ITO/PEDOT:PSS (50 nm)/dendrimer (45 nm)/DPSF (50 nm)/LiF (0.5 nm)/Al (100 nm) were firstly fabricated (Fig. 7). In this case, DPSF (2,7-bis(diphenylphosphoryl)-9,9'-spirobifluorene) was used as the electron-transporting and hole-blocking material³⁸. The corresponding EL spectra at a driving voltage of 8 V are illuminated in Fig. 8. All the dendrimers emit strong electrophosphorescence from the Ir core, whose profiles seem to be different from the PL counterparts in solid states (Fig. 4b). This is probably attributed to different excitation environment and microcavity effect in OLEDs.³⁹⁻⁴⁰ From **Ir-G1B** to **Ir-G3B**, a 4 nm hypsochromic shift is observed for their emission maxima associated with a weakened shoulder at about 500 nm. As a result, the Commission International de L'Eclairage (CIE 1931) coordinates are blue-shifted from (0.23, 0.46) of **Ir-G1B** to (0.25,

**Fig. 7** Schematic diagram of EL device configuration, the molecular structure and energy levels of the relevant materials used in the device.

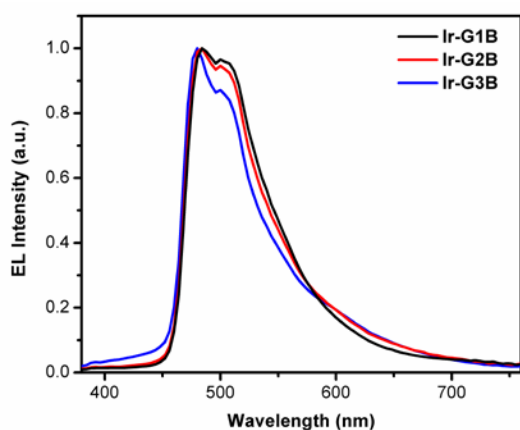


Fig. 8 EL spectra of Ir dendrimers at a driving voltage of 8 V.

0.35) of **Ir-G3B**. The CIE variation again suggests the inhibited intermolecular interactions in **Ir-G3B**.

Fig. 9 shows the current density-voltage-brightness characteristics as well as the luminous efficiency and external quantum efficiency (EQE) as a function of current density. The turn-on voltage of **Ir-G1B** is 4.6 V, which is gradually decreased to 4.2 and 3.9 V for **Ir-G2B** and **Ir-G3B**, respectively. As discussed above, this observation can be explained by the smaller hole injection barrier of **Ir-G2B** and **Ir-G3B** relative to **Ir-G1B**. In addition, the maximum luminous efficiency and EQE are enhanced from 4.7 cd/A and 1.8% of **Ir-G1B** to 9.2 cd/A and 3.8% of **Ir-G3B**, respectively. The obtained improvement is mainly due to the reduced luminescence quenching induced by the effective isolation from the dendritic wedge. We note that these values are still lower than that of a previously-reported blue-emitting dendrimer **B-G2** with a similar structure.³⁵ The different linking position between Ir core and dendrons, which would affect the encapsulation density and photophysical property, may contribute to the poor nondoped device performance.⁴¹⁻⁴² The related investigation as well as the effort to directly synthesize *p*-HO-dfppyIr and its corresponding Ir dendrimers is under way.

The device performance of the dendrimers can be further optimized by dispersing them into a dendritic host H2. The optimal doping concentration is 20 wt% for **Ir-G1B** and 40 wt% for **Ir-G2B** and **Ir-G3B**. As can be clearly seen from Fig. 9 and Table 2, the turn-on voltages of doped devices lower down to 3.4-4.0 eV, and their luminous efficiencies rise up to 20.0-25.2 cd/A, which is about 2-5 times higher than that of nondoped devices. Different from nondoped ones, it should be noted that, the luminous efficiency of doped devices monotonically

Table 2. Device performance of Ir dendrimers.

	V_{on}^a [V]	L_{max}^b [cd/m ²]	$\eta_{ext, max}^c$ [%]	$\eta_{c, max}^d$ [cd/A]	$\eta_{p, max}^e$ [lm/W]	CIE ^f (x, y)
Ir-G1B	4.6	420	1.8	4.7	3.0	(0.23, 0.46)
Ir-G2B	4.2	298	2.5	5.9	4.3	(0.24, 0.41)
Ir-G3B	3.9	221	3.8	9.2	6.9	(0.25, 0.35)
Ir-G1B (20 wt %)	3.4	1388	9.7	25.2	23.3	(0.20, 0.46)
Ir-G2B (40 wt %)	3.4	851	9.7	24.9	21.4	(0.20, 0.46)
Ir-G3B (40 wt %)	4.0	783	8.2	20.0	15.7	(0.20, 0.43)

^a At a brightness of 1 cd/m²; ^b Maximum brightness; ^c Maximum external quantum efficiency; ^d Maximum current efficiency; ^e Maximum power efficiency; ^f Data measured at a driving voltage of 8 V

decreases with the increasing generation. We propose that the concentration quenching in a doped device is not the critical factor to determine the device performance any longer. Actually, the large intercore distance in a high generation Ir dendrimer would deteriorate charge transport and recombination of the emissive layer. Therefore, **Ir-G1B** with the smallest dendrons delivers the best doped device performance among **Ir-G1B** ~ **Ir-G3B**.

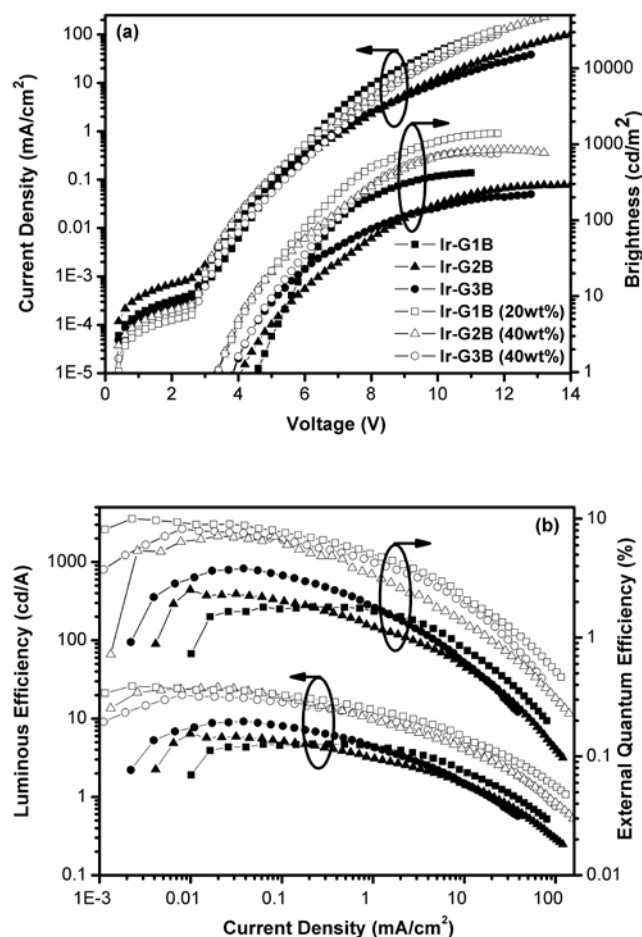


Fig. 9 The current density and brightness versus voltage (a), as well as luminous efficiency and EQE versus current density characteristics (b) of nondoped and doped electrophosphorescent devices for Ir dendrimers.

Cite this: DOI: 10.1039/c0xx00000x

www.rsc.org/xxxxxx

ARTICLE TYPE

Conclusions

In conclusion, a convenient post-dendronization method has been demonstrated for the development of solution processible greenish-blue-emitting Ir dendrimers with polyether dendrons made of NPC. Since the possible existed resonance structure between enol and keto that is induced by the hydroxyl position has a great effect on the coordination reaction, *m*-HO-dfppyIr with three reactive hydroxyl groups at meta position relative to N atom is successfully synthesized, which is then attached to NPC-containing polyether dendrons to afford Ir dendrimers with the first, second and third generation (**Ir-G1B**, **Ir-G2B** and **Ir-G3B**) in high yields over 60%. They all show not only good thermal stability with high decomposition (> 380 °C) and glass transition temperatures (> 200 °C), but also strong phosphorescence from emissive Ir core with promising luminous efficiencies up to 20.0-25.2 cd/A. Owing to the compatibility with the structural modification, we believe that, this post-dendronization procedure would be easily extended to other emission colors by tailoring the central core and dendritic wedge.

Experimental

General information

All chemicals and reagents were used as received from commercial sources without further purification. Solvents for chemical synthesis were purified according to the standard procedures. **Dn-Br** (n = 1, 2 and 3) were prepared according to our previous work.³⁶ Poly(3,4-ethylenedioxythiophene): Poly(styrenesulfonate) (PEDOT:PSS) was obtained from H. C. Starck Baytron. DPSF was prepared in our lab following a literature method.³⁸ ¹H and ¹⁹F NMR spectra were recorded with Bruker Avance NMR spectrometers. Elemental analysis was performed using a Bio-Rad elemental analysis system. MALDI-TOF mass spectra were performed on an AXIMA CFR MS apparatus (COMPACT) using 2-[(2*E*)-3-(4-*tert*-butylphenyl)-2-methylprop-2-enylidene-*ne*] malononitrile (DCTB) as the matrix.

Photophysical characterization

The UV/Vis absorption and photoluminescence spectra were measured by a Perkin-Elmer Lambda 35 UV/Vis spectrometer and a Perkin-Elmer LS 50B spectrofluorometer, respectively. Solution spectra were recorded in dichloromethane for UV/Vis absorption with a concentration of 10⁻⁶ M and toluene for photoluminescence with a concentration of 10⁻⁵ M. Thin films on quartz for spectroscopic measurements were prepared by drop-coating. All the above experiments and measurements were carried out at room temperature under ambient conditions. Solution PL quantum efficiency was measured in Ar-saturated toluene by a relative method using *fac*-Ir(ppy)₃ (Φ_p = 0.40 in toluene) as the standard.²⁶ The lifetimes of phosphorescence from the samples were measured in Ar atmosphere by exciting the samples with 355 nm light pulses with ca. 3 ns pulse width from a

Quanta-Ray DCR-2 pulsed Nd:YAG laser. The lifetimes measured in solid films were obtained by a biexponential fit of emission decay curves, and average lifetimes could be calculated according to the equation: $\tau_{av} = (A_1\tau_1^2 + A_2\tau_2^2)/(A_1\tau_1 + A_2\tau_2)$.

Cyclic voltammetry

All measurements were carried out in dichloromethane with a conventional three-electrode system consisting of a platinum working electrode, a platinum counter electrode, and an Ag/AgCl reference electrode. The supporting electrolyte was 0.1 M tetrabutylammonium perchlorate (*n*-Bu₄NClO₄). All potentials were calibrated against the ferrocene/ferrocenium couple (Fc/Fc⁺). The HOMO levels were calculated according to the equation HOMO = -e [E_{ox} + 4.8 V], where E_{ox} was the initial oxidation peak value,²⁸ and the LUMO levels were calculated according to the equation LUMO = HOMO + ΔE_g, where ΔE_g is the optical band gap estimated from the onset of the absorption spectrum.³³

Device fabrication and testing

To fabricate OLEDs, a 50-nm-thick PEDOT:PSS film was first deposited on the pre-cleaned ITO-glass substrates (20 Ω per square) and subsequently baked at 120 °C for 40 min. Then, solutions of the dendrimers or mixture of dendrimers and H2 in chlorobenzene with a concentration of 10 mg/ml were spin-coated onto PEDOT:PSS at a speed of 1200 r/min as the emissive layer (EML). The thickness of the EML was about 45 nm. Successively, a 50-nm-thick film of DPSF was thermally evaporated on top of the EML at a base pressure less than 10⁻⁶ Torr (1 Torr = 133.32 Pa). Finally, 0.5 nm LiF and 100 nm Al were deposited as the cathode through a shadow mask with an array of 14 mm² openings. The EL spectra and CIE coordinates were measured using a PR650 spectra colorimeter. The current-voltage and brightness-voltage curves of devices were measured using a Keithley 2400/2000 source meter and a calibrated silicon photodiode. All the measurements were carried out at room temperature under ambient conditions.

Synthesis of 2-(2',4'-difluorophenyl)-5-hydroxypyridine (HO-dfppy)

A mixture of 2-bromo-5-hydroxypyridine (3.5 g, 20.0 mmol), 2,4-difluorophenylboronic acid (5.1 g, 32.0 mmol), Pd(PPh₃)₄ (693 mg, 0.6 mmol) in 50 mL THF and 30 mL 2 M Na₂CO₃ aqueous solution was heated at 70 °C for 12 h under argon. The mixture was extracted with CH₂Cl₂ and dried over anhydrous Na₂SO₄. The product was purified by column chromatography on silica gel using ethyl acetate: petroleum ether = 1:5 as eluent to give a white solid. Yield: 96%. ¹H NMR (400 MHz, d₆-DMSO) [ppm]: δ 10.18 (s, 1H), 8.26 (d, J = 2.8 Hz, 1H), 7.92 (dt, J = 9.0, 9.0, 7.1 Hz, 1H), 7.61 (dd, J = 8.6, 1.9 Hz, 1H), 7.34 (ddd, J = 11.7, 9.4, 2.5 Hz, 1H), 7.27 (dd, J = 8.6, 2.9 Hz, 1H), 7.18 (dt, J = 8.5, 8.5, 2.3 Hz, 1H).

Synthesis of *m*-HO-dfppyIr

IrCl₃•3H₂O (1.8 g, 5.0 mmol) and HO-dfppy (2.2 g, 10.5 mmol) were added in a 160 mL mixture of 2-methoxyethanol (120 mL) and water (40 mL). The mixture was refluxed for 24 h and then poured into water. The solid was collected by filtration and dried in vacuum to give crude chloro-bridged dimer complex. Without further purification, the dimer was added in a mixture of silver trifluoroacetate (1.2 g, 5.5 mmol), HO-dfppy (1.3 g, 6.3 mmol), 2-ethoxyethanol (100 mL). After heated at reflux for 24 h, the mixture was poured into water, filtered, washed with water and dried in vacuum. The *mer*-isomer product was obtained by chromatography on silica gel using CH₂Cl₂: ethyl acetate = 15:1 as eluent and then transformed into *fac*-isomer product in methanol using a 125 W UV lamp for 8 h. Finally, the pure *fac*-isomer product was obtained by chromatography on silica gel using CH₂Cl₂: ethyl acetate = 1:1 as eluent in a total yield of 25%. ¹H NMR (400 MHz, d₆-DMSO) [ppm]: δ 10.39 (s, 3H), 8.09 (d, J = 10.1 Hz, 3H), 7.38 (dd, J = 8.9, 2.5 Hz, 3H), 7.11 (d, J = 2.6 Hz, 3H), 6.78-6.46 (m, 3H), 5.98 (dd, J = 9.1, 2.4 Hz, 3H). ¹⁹F NMR (376 MHz, d₆-DMSO, δ (vs. fluorobenzene)): 1.6 (d, J = 8.3 Hz, 3F), 0.1 (d, J = 8.2 Hz, 3F). MALDI-TOF MS: calcd for C₃₃H₁₈F₆IrN₃O₃: 811.1 found: 811.1 [M⁺]. Anal. calcd for C₃₃H₁₈F₆IrN₃O₃: C 48.89, H 2.24, N 5.18 Found: C 49.00, H 2.32, N 5.10.

General procedure for the synthesis of Ir-GnB

To a solution of *m*-HO-dfppyIr (1 equiv) and Cs₂CO₃ (3.3 equiv) in DMF (5 mL) were added **Dn-Br** (3.3 equiv) (The concentration of mixture is 100 mg/mL). After heated at 100 °C for 12 h, the mixture was poured into water, extracted with dichloromethane. The organic layer was carefully washed with water and dried with Na₂SO₄. The crude product was purified by chromatography on silica gel using petroleum ether: CH₂Cl₂ = 3:1 as eluent.

Ir-G1B: Yield: 70%. ¹H NMR (400 MHz, CDCl₃) [ppm]: δ 8.28 (d, J = 9.7 Hz, 3H), 8.10 (s, 6H), 7.37-7.29 (m, 15H), 7.19-7.11 (m, 15H), 6.43-6.38 (m, 3H), 6.19 (d, J = 9.1 Hz, 3H), 4.77 (s, 6H), 1.41 (s, 54H). ¹⁹F NMR (376 MHz, CDCl₃, δ (vs. fluorobenzene)): 3.17 (d, J = 8.9 Hz, 3F), 0.43 (d, J = 8.6 Hz, 3F). MALDI-TOF MS: calcd for C₁₁₄H₁₀₅F₆IrN₆O₃: 1913.3 found: 1913.3 [M⁺]. Anal. calcd for C₁₁₄H₁₀₅F₆IrN₆O₃: C, 71.56; H, 5.53; N, 4.39. Found: C, 71.47; H, 5.71; N, 4.30.

Ir-G2B: Yield: 65%. ¹H NMR (400 MHz, CDCl₃) [ppm]: δ 8.32 (d, J = 11.6 Hz, 3H), 8.11 (br, 12H), 7.67 (br, 6H), 7.60-7.57 (m, 12H), 7.52-7.49 (m, 12H), 7.40-7.37 (m, 15H), 7.29-7.27 (m, 18H), 7.20-7.18 (m, 9H), 7.14 (d, J = 8.9 Hz, 6H), 7.07 (d, J = 9.0 Hz, 6H), 6.54-6.31 (m, 3H), 6.21 (d, J = 8.5 Hz, 3H), 5.16 (s, 12H), 4.81 (s, 6H), 1.42 (s, 108H). ¹⁹F NMR (376 MHz, CDCl₃, δ (vs. fluorobenzene)): 3.42 (d, J = 9.1 Hz, 3F), 0.55 (d, J = 8.9 Hz, 3F). MALDI-TOF MS: calcd for C₂₅₂H₂₃₁F₆IrN₁₂O₉: 3877.8 found: 3877.8 [M⁺]. Anal. calcd for C₂₅₂H₂₃₁F₆IrN₁₂O₉: C, 78.05; H, 6.00; N, 4.33. Found: C, 77.81; H, 6.10; N, 4.30.

Ir-G3B: Yield: 60%. ¹H NMR (400 MHz, CDCl₃) [ppm]: δ 8.32 (d, J = 11.4 Hz, 3H), 8.11 (br, 24H), 7.67 (br, 24H), 7.63-7.46 (m, 72H), 7.41-7.38 (m, 27H), 7.31-7.28 (m, 33H), 7.24-7.21 (m, 6H), 7.16-7.13 (m, 9H), 7.10-7.03 (m, 21H), 6.45-6.39 (m, 3H), 6.20 (d, J = 8.8 Hz, 3H), 5.30-5.28 (m, 6H), 5.5.17-5.10 (m, 36H), 1.42 (m, 216H). ¹⁹F NMR (376 MHz, CDCl₃, δ (vs. fluorobenzene)): 3.51 (d, J = 9.2 Hz, 3F), 0.67 (d, J = 8.8 Hz, 3F). MALDI-TOF MS: calcd for C₅₂₈H₄₈₃F₆IrN₂₄O₂₁: 7806.8 found:

7806.8 [M⁺]. Anal. calcd for C₅₂₈H₄₈₃F₆IrN₂₄O₂₁: C, 81.23; H, 6.24; N, 4.31. Found: C, 81.20; H, 6.30; N, 4.28.

Notes and references

- ^a State Key Laboratory of Polymer Physics and Chemistry, Changchun Institute of Applied Chemistry, Chinese Academy of Sciences, Changchun 130022, P. R. China E-mail: junqiaod@ciac.ac.cn; lixiang@ciac.ac.cn
- ^b University of Chinese Academy of Sciences, Beijing, 100049, P. R. China
- M. A. Baldo, D. F. O'Brien, Y. You, A. Shoustikov, S. Sibley, M. E. Thompson and S. R. Forrest, *Nature*, 1998, **395**, 151.
 - M. A. Baldo, D. F. O'Brien, M. E. Thompson and S. R. Forrest, *Phys. Rev. B*, 1999, **60**, 14422.
 - S. Lamansky, P. Djurovich, D. Murphy, F. Abdel-Razzaq, H. E. Lee, C. Adachi, P. E. Burrows, S. R. Forrest and M. E. Thompson, *J. Am. Chem. Soc.*, 2001, **123**, 4304.
 - P. Furuta, J. Brooks, M. E. Thompson and J. M. J. Fréchet, *J. Am. Chem. Soc.*, 2003, **125**, 13165.
 - (a) C. L. Ho, W. Y. Wong, Z. Q. Gao, C. H. Chen, K. W. Cheah, B. Yao, Z. Y. Xie, Q. Wang, D. G. Ma, L. A. Wang, X. M. Yu, H. S. Kwok and Z. Y. Lin, *Adv. Funct. Mater.*, 2008, **18**, 319; (b) L. Ying, C. L. Ho, H. B. Wu, Y. Cao and W. Y. Wong, *Adv. Mater.*, 2014, **26**, 2459; (c) X. L. Yang, G. J. Zhou and W. Y. Wong, *J. Mater. Chem. C*, 2014, **2**, 1760; (d) G. J. Zhou, W. Y. Wong and S. Suo, *J. Photoch. Photobio. C*, 2010, **11**, 133.
 - T. Sajoto, P. I. Djurovich, A. B. Tamayo, J. Oxgaard, W. A. Goddard and M. E. Thompson, *J. Am. Chem. Soc.*, 2009, **131**, 9813.
 - C. Adachi, M. A. Baldo, M. E. Thompson and S. R. Forrest, *J. Appl. Phys.*, 2001, **90**, 5048.
 - T. Tsuzuki, Y. Nakayama, J. Nakamura, T. Iwata and S. Tokito, *Appl. Phys. Lett.*, 2006, **88**, 243511.
 - (a) C. H. Fan, P. P. Sun, T. H. Su and C. H. Cheng, *Adv. Mater.*, 2011, **23**, 2981; (b) W. Y. Wong and C. L. Ho, *Coord. Chem. Rev.*, 2009, **253**, 1709.
 - Y. T. Tao, Q. A. Wang, C. L. Yang, C. Zhong, J. G. Qin and D. G. Ma, *Adv. Funct. Mater.*, 2010, **20**, 2923.
 - H. Sasabe, H. Nakanishi, Y. Watanabe, S. Yano, M. Hirasawa, Y. J. Pu and J. Kido, *Adv. Funct. Mater.*, 2013, **23**, 5550.
 - M. S. Lin, S. J. Yang, H. W. Chang, Y. H. Huang, Y. T. Tsai, C. C. Wu, S. H. Chou, E. Mondal and K. T. Wong, *J. Mater. Chem.*, 2012, **22**, 16114.
 - H. H. Chou and C. H. Cheng, *Adv. Mater.*, 2010, **22**, 2468.
 - X. W. Chen, J. L. Liao, Y. M. Liang, M. O. Ahmed, H. E. Tseng and S. A. Chen, *J. Am. Chem. Soc.*, 2003, **125**, 636.
 - A. J. Sandee, C. K. Williams, N. R. Evans, J. E. Davies, C. E. Boothby, A. Kohler, R. H. Friend and A. B. Holmes, *J. Am. Chem. Soc.*, 2004, **126**, 7041.
 - X. Gong, M. R. Robinson, J. C. Ostrowski, D. Moses, G. C. Bazan and A. J. Heeger, *Adv. Mater.*, 2002, **14**, 581.
 - G. X. Jiang, C. L. Bian, J. Q. Ding and L. X. Wang, *Chinese. J. Polym. Sci.*, 2013, **31**, 787.
 - C. Fan, Y. H. Li, C. L. Yang, H. B. Wu, J. G. Qin and Y. Cao, *Chem Mater.*, 2012, **24**, 4581.
 - P. L. Burn, S. C. Lo and I. D. W. Samuel, *Adv. Mater.*, 2007, **19**, 1675.
 - S. H. Hwang, C. N. Moorefield and G. R. Newkome, *Chem. Soc. Rev.*, 2008, **37**, 2543.
 - J. Y. Li and D. Liu, *J. Mater. Chem.*, 2009, **19**, 7584.
 - S. C. Lo, T. D. Anthopoulos, E. B. Namdas, P. L. Burn and I. D. W. Samuel, *Adv. Mater.*, 2005, **17**, 1945.
 - S. C. Lo, R. N. Bera, R. E. Harding, P. L. Burn and I. D. W. Samuel, *Adv. Funct. Mater.*, 2008, **18**, 3080.
 - S. C. Lo, R. E. Harding, C. P. Shipley, S. G. Stevenson, P. L. Burn and I. D. W. Samuel, *J. Am. Chem. Soc.*, 2009, **131**, 16681.
 - W. S. Huang, J. T. Lin and H. C. Lin, *Org. Electron.*, 2008, **9**, 557.
 - T. S. Qin, J. Q. Ding, L. X. Wang, M. Baumgarten, G. Zhou and K. Müllen, *J. Am. Chem. Soc.*, 2009, **131**, 14329.

- 27 G. J. Zhou, W. Y. Wong, B. Yao, Z. Y. Xie and L. X. Wang, *Angew. Chem. Int. Ed.*, 2007, **46**, 1149.
- 28 M. R. Zhu, J. H. Zou, X. He, C. L. Yang, H. B. Wu, C. Zhong, J. G. Qin and Y. Cao, *Chem. Mater.*, 2012, **24**, 174.
- 5 29 B. Liang, L. Wang, Y. Xu, H. Shi and Y. Cao, *Adv. Funct. Mater.*, 2007, **17**, 3580.
- 30 M. R. Zhu, Y. H. Li, S. J. Hu, C. G. Li, C. L. Yang, H. B. Wu, J. G. Qin and Y. Cao, *Chem. Commun.*, 2012, **48**, 2695.
- 31 (a) J. Q. Ding, J. Gao, Y. X. Cheng, Z. Y. Xie, L. X. Wang, D. G. Ma, X. B. Jing and F. S. Wang, *Adv. Funct. Mater.*, 2006, **16**, 575; (b) Y. Zou, J. H. Zou, T. L. Ye, H. Li, C. L. Yang, H. B. Wu, D. G. Ma, J. G. Qin and Y. Cao, *Adv. Funct. Mater.*, 2013, **23**, 1781.
- 10 32 T. Tsuzuki, N. Shirasawa, T. Suzuki and S. Tokito, *Jpn. J. Appl. Phys.*, 2005, **44**, 4151.
- 15 33 J. Q. Ding, J. H. Lu, Y. X. Cheng, Z. Y. Xie, L. X. Wang, X. B. Jing and F. S. Wang, *Adv. Funct. Mater.*, 2008, **18**, 2754.
- 34 L. C. Chen, Z. H. Ma, J. Q. Ding, L. X. Wang, X. B. Jing and F. S. Wang, *Org. Electron.*, 2012, **13**, 2160.
- 35 (a) D. B. Xia, B. Wang, B. Chen, S. M. Wang, B. H. Zhang, J. Q. Ding, L. X. Wang, X. B. Jing and F. S. Wang, *Angew. Chem. Int. Ed.*, 2014, **53**, 1048; (b) W. Y. Wong and C. L. Ho, *J. Mater. Chem.*, 2009, **19**, 4457; (c) G. J. Zhou, W. Y. Wong and X. L. Yang, *Chem.-Asian. J.*, 2011, **6**, 1706.
- 20 36 Y. Wang, S. M. Wang, N. Zhao, B. X. Gao, S. Y. Shao, J. Q. Ding, L. X. Wang, X. B. Jing and F. S. Wang, unpublished.
- 25 37 A. B. Tamayo, B. D. Alleyne, P. I. Djurovich, S. Lamansky, I. Tsyba, N. N. Ho, R. Bau and M. E. Thompson, *J. Am. Chem. Soc.*, 2003, **125**, 7377.
- 38 K. S. Yook, S. E. Jang, S. O. Jeon and J. Y. Lee, *Adv. Mater.*, 2010, **22**, 4479.
- 30 39 Z. X. Wu, L. D. Wang, G. T. Lei and Y. Qiu, *J. Appl. Phys.*, 2005, **97**, 103105.
- 40 J. Q. Ding, J. Gao, Q. Fu, Y. X. Cheng, D. G. Ma and L. X. Wang, *Synth. Met.*, 2005, **155**, 539.
- 35 41 J. Q. Ding, B. Wang, Z. Y. Yue, B. Yao, Z. Y. Xie, Y. X. Cheng, L. X. Wang, X. B. Jing and F. S. Wang, *Angew. Chem. Int. Edit.*, 2009, **48**, 6664.
- 42 J. Q. Ding, J. H. Lu, Y. X. Cheng, Z. Y. Xie, L. X. Wang, X. B. Jing and F. S. Wang, *J. Organomet. Chem.*, 2009, **694**, 2700.